A Comprehensive Study of the Active Site Residues of DT-Diaphorase: Rational Design of Benzimidazolediones as DT-Diaphorase Substrates†

Ali Suleman and Edward B. Skibo*

Department of Chemistry and Biochemistry, Arizona State University, Tempe, Arizona 85287-1604

Received September 17, 2001

A series of quinone substrates were modeled into the active site of human DT-diaphorase and minimized. Correlation of these models with the substrate specificity k_{cat}/K_m provided insights into the structural requirements of quinone substrates. The W105, F106, and H194 residues can influence the position of the quinone substrate in the active site resulting in formation of one of the two possible Michael anions resulting from hydride transfer from $FADH_2$. Electron withdrawing groups on the substrate can stabilize these anions resulting in excellent substrate specificity. Inspection of models indicated that the W-105 and F-106 residues form parallel walls that will accommodate large polycyclic substrates. Thus excellent polycyclic substrates of DT-diaphorase were designed. However, the placement of tetrahedral centers on these polycyclic substrates interfered with the W-105 and the F-106 residues resulting in their exclusion from the active site. The histidine (H194) residue permits recognition of substrate enantiomers as a result of hydrogen bonding interactions. As a result of this study, it will be possible to design poor to excellent substrates of DT-diaphorase and take advantage of varying levels of this enzyme in histologically different cancers.

The enzyme DT-diaphorase is an NADPH-dependent reducing enzyme that reduces quinones and other substrates to the corresponding two-electron reduction products. This enzyme is elevated in some cancers, and the reduction process can lead to either activation or inactivation of antitumor agents, Chart 1.[1−4] The reductive activation process is well-known with substrates such as mitomycin C,[5,6] indoloquinones,[7,8] and the PBIs,[9,10] which are converted to the corresponding cytotoxic hydroquinones. In contrast, some environmental toxins[1,11−13] and the APBI antitumor agents[9,14] are inactivated upon DT-diaphorase reduction. A recent report from this laboratory revealed that the level of substrate specificity for DT-diaphorase influences cytotoxicity, cancer specificity, and in vivo toxicity.[15] The rational design of DT-diaphorase substrates is therefore essential to take advantage of DT-diaphorase levels in cancers and control toxicity.

In the present study, molecular modeling and substrate specificity determinations were performed with the diverse quinone systems developed in this laboratory over the years. These systems are all benzimidazole-based quinones but vary with respect to size (tricyclic to pentacyclic), stereochemistry, and substituents. From these models it was possible to gain insights into the mechanism of DT-diaphorase reduction as well as the role of amino acid residues in the active site. The models developed in this study will be used to develop new DT-diaphorase activated antitumor agents.

Chart 1

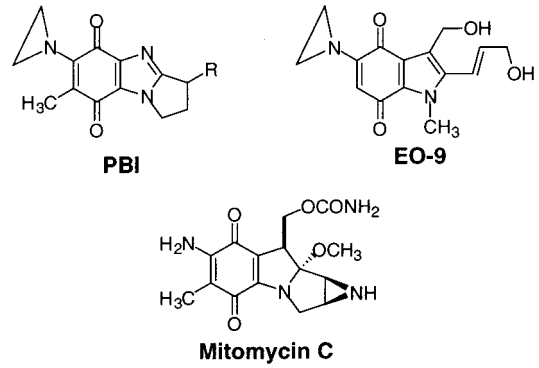

Results and Discussion

Quinone Substrates and Their Preparation. The quinone substrates **1**−**5** shown in Chart 2 represent a structurally diverse series of benzimidazole-based compounds that permitted the development of a computer model able to predict substrate specificity. We maintained the benzimidazole structure throughout the series so as to keep the quinone redox potentials within the same range. Variables include stereochemistry, hydrogen bonding capability, and substrate dimension.

The preparation of series **1a**−**c** was recently reported,[16] and the new analogue **1d** was readily prepared by the reaction of **1a** with *N*,*N*-dimethylcarbamyl chloride. Series **2** represents the tetrahydropyrido version of series **1**. Access to both enantiomers of **2** in pure form was possible starting with (D) or (L) 2,5-diaminopentanoic acid as outlined in Scheme 1. The synthetic methodology outlined in Scheme 1 has been described

† Abbreviations: TMS, tetramethylsilane; TLC, thin layer chromatography; HPLC, high performance liquid chromatography; PDB, protein data bank; CVFF, consistent valence force field; RMSD, root mean square distance; FAD, flavin adenine dinucleotide; $FADH_2$, flavin adenine dinucleotide reduced; NAD^+, nicotinamide adenine dinucleotide; NADH, Nicotinamide adenine dinucleotide reduced; NADPH, nicotinamide adenine dinucleotide phosphate reduced; NSC non-small-cell.

* To whom correspondence should be addressed. Telephone: 480-965-3581. Fax: 480-965-2747. E-mail: ESkibo@ASU.ed.

10.1021/jm0104365 CCC: $22.00
Published on Web 02/09/2002

Chart 2

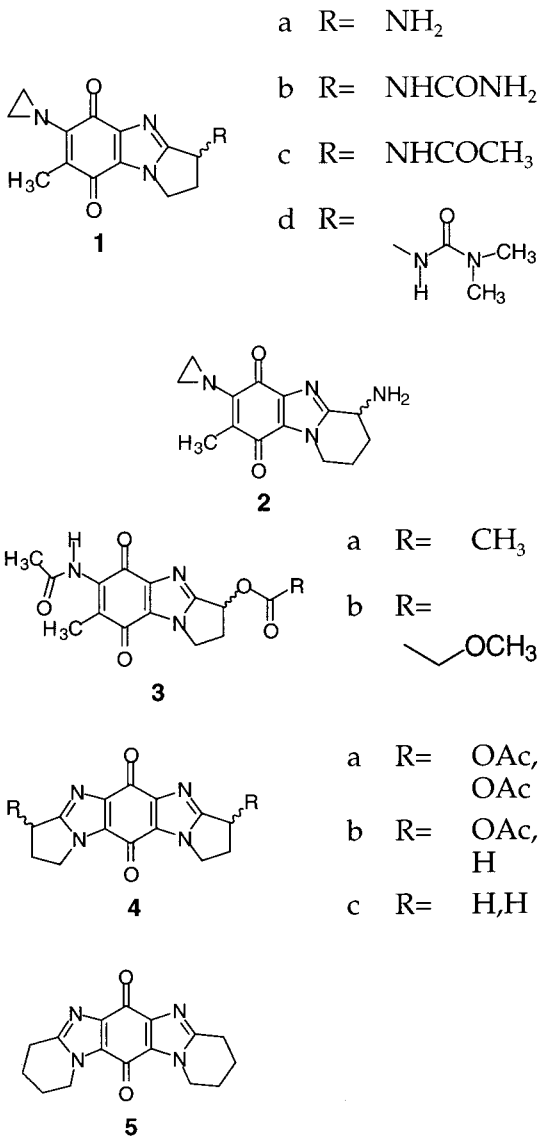

in the literature.[16,17] The enantiomerically pure forms of series **3**[9] and **4**[14] were carried out as reported in the literature. The preparation of **5** involved the double annulation methodology illustrated in Scheme 2.

Modeling of Substrates into the Human DT-Diaphorase Active Site and Substrate Specificity (k_{cat}/K_m) Determinations. This section discusses the generation of quinone substrate models in the human DT-diaphorase active site employing the crystal structure of rat DT-diaphorase. The rat enzyme crystal structure has a duroquinone substrate bound to the active site whereas the human enzyme has no quinone substrate. Models of the human DT-diaphorase active site bearing quinone substrates were generated by a series of superimpositions and minimizations described in the Experimental Section. In addition, active site energies of enzyme-bound substrates were determined and correlated with measured values of substrate specificity.

The active site of DT-diaphorase has been defined from crystal structures as well as from substrate studies of both rat and human enzymes.[18−20] Human DT-diaphorase (from non-small cell lung NCI-H460) has been cloned[18] and its crystal structure determined

Scheme 1

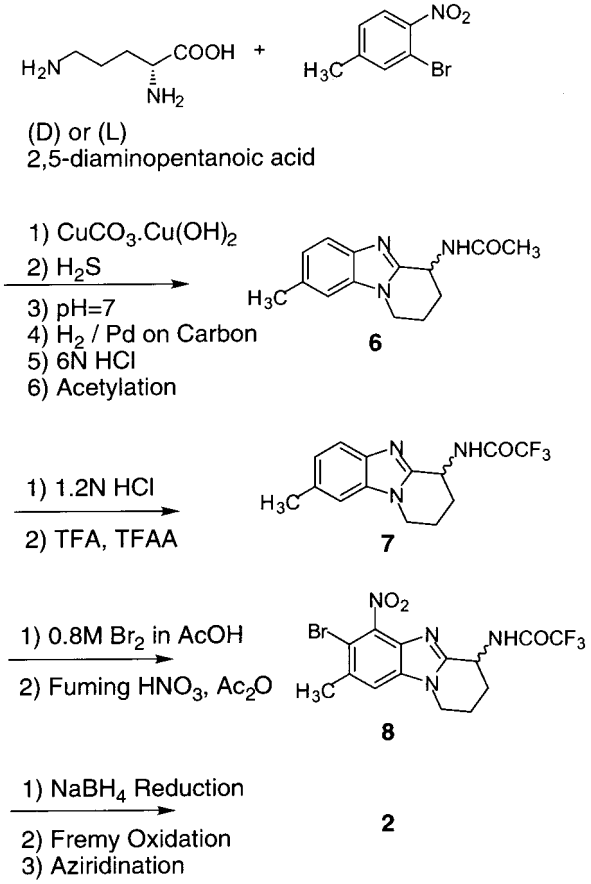

Scheme 2

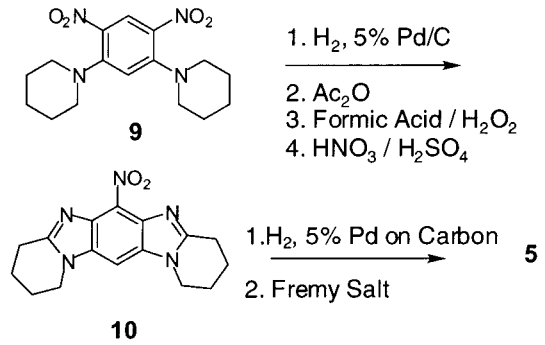

(1D4A). Previously, studies of substrate reductions by human and rat DT-diaphorases have been carried out employing computer modeling into crystal structures.[19,21−23]

From computer-generated models of the respective active sites shown in Figure 1, the human diaphorase active site is more compact than the rat enzyme active site in that W105 and H194 are closer to each other. These models show that the His-194 residue in human model is closer to the other active site residues than the rat model and therefore better able to undergo hydrogen bonding interactions with substrates.[24] Since the positions of the important active site residues (other than His 194) are similar for both enzymes, superimposition of the duroquinone substrate complex of rat enzyme into the human active site is feasible.

The superimposition process is described below:

First, the quinone ring of **1**−**4** was superimposed onto the duroquinone ring of the minimized A-chain of the

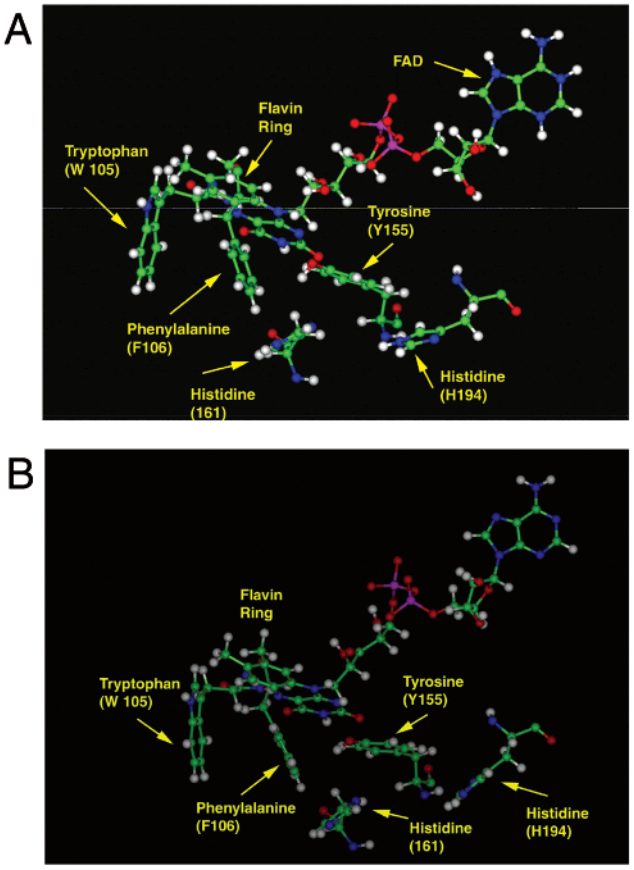

Figure 1. Active sites of (A) human cancer (from NCI-H460 non-small-lung**)** and (B) rat DT-diaphorase from the protein database, 1D4A and 1QRD. Important amino acid residues are labeled.

1QRD dimer. There are two to four ways to superimpose **1**−**4** on duroquinone, so each possible superimposition was made and the lowest energy structure was chosen for the next step. The superimposition with the lowest energy was chosen as the most likely substrate/enzyme complex structure. This process correctly predicted that **4a** cannot be a DT-diaphorase substrate since none of the possible superimpositions afforded a stable structure. In contrast, the most stable superimposed structures of **1**−**2** show the aziridinyl ring in the same position as that of EO9 in the DT-diaphorase active site.[23]

Second, the 1QRD:A chain bearing the new quinone substrate was added to the 1D4A:A crystal structure by superimposition of the FAD cofactors. After deleting the 1QRD:A chain and the rat FAD, the optimal binding orientation of the 1D4A:A chain with the quinone substrate was then minimized utilizing the consistent valence force field (CVFF). The minimization was either carried out for 5000 iterations or until RMS of less than 0.05 was reached.

Third, electrostatic and van der Waals energies (active site energies) were calculated for the active site residues (W-105, F-106, Y-155, H-161, H-194) along with the FAD cofactor and the superimposed quinone. The energies obtained from the 5000 iteration minimization are listed in Table 1.

The 1D4A:A-bound quinone structures obtained as described above were evaluated with respect to their position with respect to the FAD cofactor. The distance

Table 1. DT-Diaphorase Kinetic Parameters and Calculated Active Site Energies

compd	k_{cat}/K_m (M^{-1} s^{-1}) $\times 10^5$	k_{cat} (s^{-1})	K_m (M) $\times 10^5$	active site energy (kcal/M)	plot
1a-(*S*)	13.9	2.64	0.19	−105	A
1a-(*R*)	6.4	3.26	0.51	−98.3	A
1b-(*R*)	8.9	2.7	0.3	−111	A
1b-(*S*)	12	2.4	0.2	−116	A
1c-(*R*)	9.2	1.47	0.16	−108	A
1c-(*S*)	5.2	1.87	0.36	−117	B
1d-(*R*)	21.3	9.56	0.45	−170	A
1d-(*S*)	9.4	3.955	0.42	−138	B
2-(*R*)	1.06	4.92	4.66	−115	B
2-(*S*)	1.88	2.972	1.58	−113	B
3a-(*R*)	1.54	3.81	1.79	−112	B
3a-(*S*)	4.72	3.85	0.59	−127	B
3b-(*R*)	0.4	4.845	12.2	−105	B
3b-(*S*)	0.69	1.735	2.5	−106	B
4c	1.18	3.811	1.18	−78	A
5	14.5	3.74	0.26	−109	A

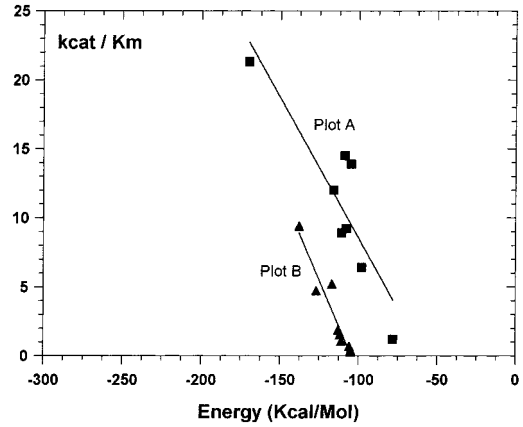

Figure 2. Plots of k_{cat}/K_m versus minimized energy (kcal/mol) for quinones **1**−**5**. The data reveal the presence of two linear plots: plot A with correlation coefficient = 0.88 and plot B with correlation coefficient = 0.95. These respective plots correspond to the two possible transition states for hydride transfer.

between the carbon center of the quinone (called "C2" in Figure 3) that would accept hydride by Michael addition and the N (5) of the isoalloxazine ring were typically 3−4 Å in models. This distance would permit hydride transfer to the quinone if the reduced cofactor were present.

The catalytic parameters for quinone substrates are also provided in Table 1. Using either k_{cat} or K_m in correlations with active site energy is risky due to the inclusion of nonproductive constants.[25] In contrast, the ratio k_{cat}/K_m provides the apparent second-order rate constant (s^{-1} M^{-1}) of the enzymatic transformation without including any nonproductive processes.

The k_{cat}/K_m versus active site energy plots shown in Figure 2 reveal a very good to excellent correlation for analogues **1**−**5** (plots A & B) when the 5000 iteration data were used. The presence of two linear plots in Figure 2, rather than one plot with a large amount of scatter may pertain to the two possible ways of hydride transfer to the quinone substrate. The linear relationships shown in Figure 2 (increasing k_{cat}/K_m with decreasing energy) is perplexing, if the calculated energy pertains to that of the enzyme substrate complex. A lower minimized energy for substrate binding will translate to an unfavorable (lower) value for k_{cat}/K_m

Scheme 3

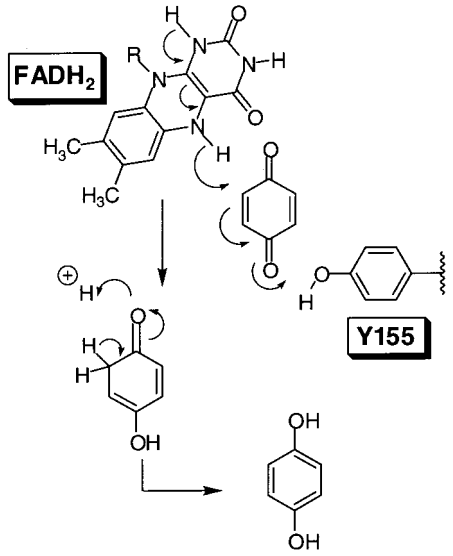

because more energy is required to reach the transition state. On the other hand, the linear relationships shown in Figure 2 can be explained if the calculated active site energy pertains to the transition state energy. The minimized active site structures, with quinone in position to accept hydride, may in fact resemble the transition state complex.

Correlation of k_{cat}/K_m with energies obtained from iteration to RMS of 0.05 afforded a zero slope plot because the active site energies of all the quinone substrates are nearly the same (110−120 kcal/mol). The quinone substrates ultimately provide similar active site structures upon complete minimization, perhaps because they are all based on the benzimidazole ring system. These minimized structures do not account for the different k_{cat}/K_m values for the substrates; therefore, they must not reflect structures on the reaction path. We conclude that minimization to RMS of less than 0.05 is not desirable, and higher energy minima actually reflect structures on the reaction path.

FAD and Tyrosine (Y 155) Residues. The tyrosine (Y 155) and histidine (H 161) residues are involved in quinone reduction when the FAD cofactor is bound in its reduced form ($FADH_2$). Previously, Li et al. suggested that hydride transfer occurs directly to the carbonyl oxygen,[20] while Schlegel et al. suggested hydride transfer directly to a quinone carbonyl carbon.[26] The former hydride transfer is not electrostatically feasible due to the electronegativity of oxygen compared to carbon. A third mechanism for quinone reduction involves hydride transfer by a Michael addition followed by tautomerization to the hydroquinone, Scheme 3.[19] In fact, this laboratory previously reported supporting evidence for hydride quinone reduction by Michael addition.[27]

The two possible hydride transfer processes shown in Scheme 4 explain the presence of two linear relationships, plots A and B in Figure 2. Inspection of the minimized structures for enzyme-bound substrates falling on plot A and plot B in Figure 3 revealed that the Michael acceptor carbon is different for each respective set of substrates. Substrates on plot B of Figure 2 possess smaller k_{cat}/K_m values than plot A because the Michael addition anions of the latter are in a more electron rich environment.

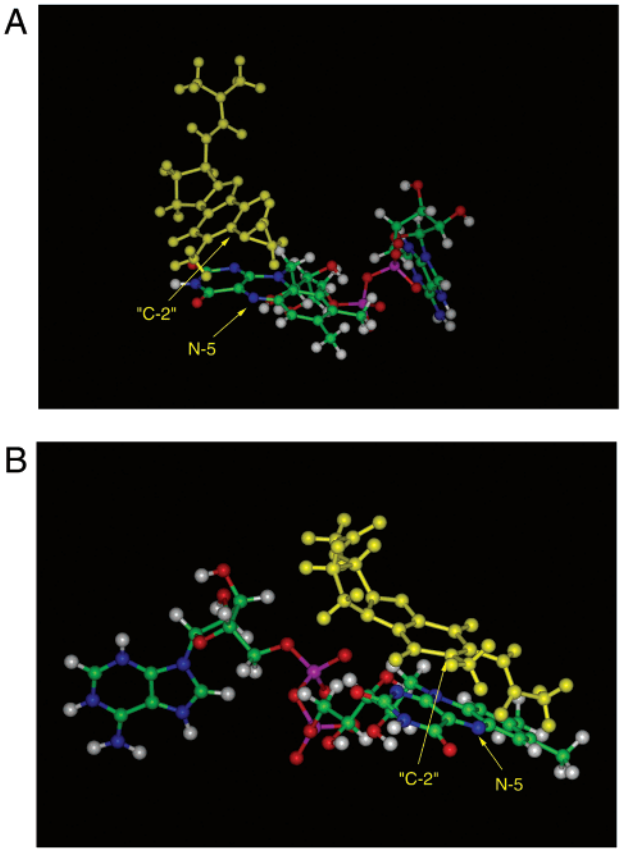

Figure 3. Inspection of molecular models of **1**−**5** revealed that plots A and B in Figure 2 are associated with different substrate orientations in the human DT-diaphorase active site. Illustrated in this figure are representative models of these two substrate orientations (A: plot A hydride attack; B: plot B hydride attack). Both active site models show the substrate in yellow with the site of hydride attack on the quinone labeled "C2" and the nitrogen bearing the hydride labeled "N-5." Note that oxidized flavin is shown in these models, and therefore a hydride is not present on N-5.

The findings cited above led to the conclusions discussed below.

Not all DT-diaphorase substrates bind like duroquinone. Thus other quinone positions with respect to the cofactor are tolerated as long as the hydride transfer could occur. Stereochemical and bulk changes are sufficient to reposition the substrate in the active site. In substrates **1**−**5**, formation of only two Michael anions is possible. The cofactor does not have access to the other two sites for hydride attack; see Scheme 4. The Y155 residue is not strictly required for the Michael addition, a conclusion previously obtained from active site mutation studies.[21] Substrates **4** and **5** are therefore reduced even though steric bulk prevents involvement of the Y155 residue. This residue may still have a catalytic role, such as in a charge relay process, but only if the substrate is too electron rich to support anion development. The Michael hydride addition mechanism can be used in the rational design of outstanding DT-diaphorase substrates. By designing a system that stabilizes the developing anion by resonance (inset of Scheme 4), we have achieved k_{cat}/K_M values of 600 M^{-1} s^{-1}. In fact, Phillips and co-workers have reported that similar 2-carbonyl substituted indoloquinones are excellent substrates for DT-diaphorase.[23]

Scheme 4

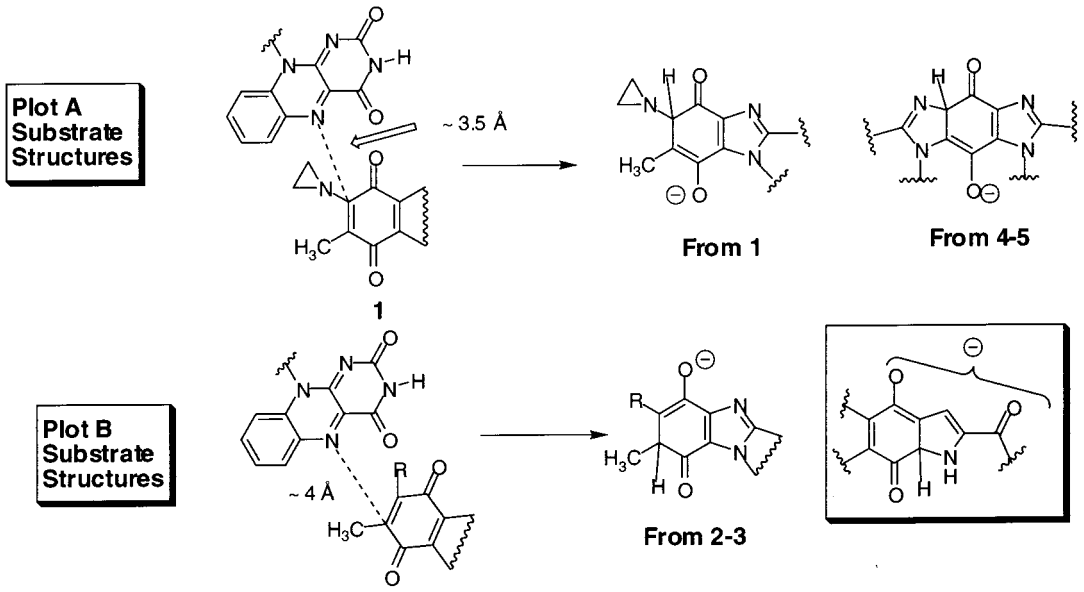

Tryptophan (W-105) and Phenylalanine (F-106) Residues. The tryptophan (W-105) and phenylalanine (F-106) residues form parallel walls by a stacking interaction. On the basis of modeling studies with the aziridinyl quinone EO9,[23] steric interactions will cause the aziridinyl ring to face away from the F-106 residue. At the same time, the aziridinyl ring will undergo hydrophobic interactions with W-105. Both W-105 and F-106 also limit the bulk of the 7-substituent of the PBI system, and substantial decreases in DT-diaphorase substrate activity have been observed when a butyl group is substituted for the methyl group normally found at the PBI 7-position.[9]

It was postulated that the tryptophan (W-105)/phenylalanine (F-106) "sandwich" could be exploited for substrate design by utilizing systems that could intercalate between these rings, Figure 4. The dipyrroloimidazobenzimidazoles **4** and dipyridoimidazobenzimidazole **5** systems were designed and found to be excellent substrates for human DT diaphorase. In addition, the analogues **4a** and **4b** were studied as systems that would be excluded from the active site by steric interactions with the tryptophan (W-105)/phenylalanine (F-106) "sandwich."

Quinones **4b**,**c** were found to be excellent substrates for human and rat DT-diaphorase while **4a** could not be reduced by either enzyme. It was concluded from the computer-generated models of active site bound **4b**,**c** that the pentacyclic quinone fitted snugly in the active site of DT-diaphorase. The binding of **4b** was such that the unsubstituted pyrrolo ring was sandwiched between the W105/F106 residues. In the case of **4a**, where both pyrrolo rings bear acetate, steric hindrance with the W105/F106 residues precluded substrate activity. Modeling studies correctly predicted that the unsubstituted pyrido derivative **5** would be an even better substrate than **4c** mainly due to increased van der Waals interactions with the W105/F106 residues.

The conclusion of this section is that DT-diaphorase can transfer electrons to large flat multi-ring systems as a result of van der Waals interactions with the W105/F106 residues. These residues very likely play the same role in the reductive detoxification of polycyclic quinones by DT-diaphorases.[12,13]

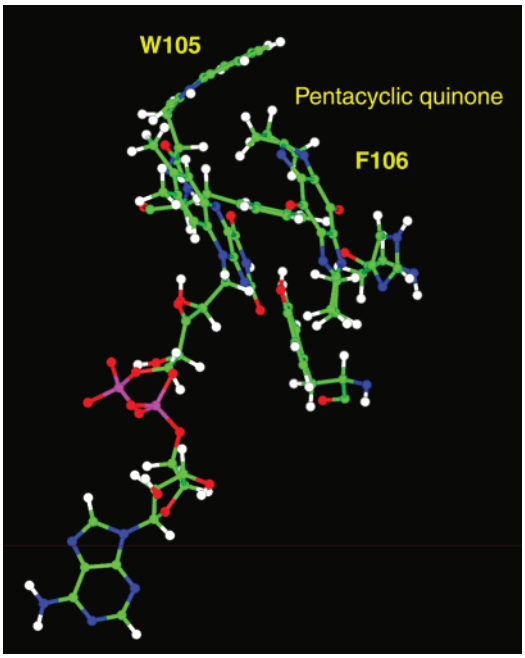

Figure 4. Quinone **4c** modeled into human DT-diaphorase active site showing the substrate sandwiched between tryptophan (W105) and phenylalanine (F106) residues.

Histidine (H194) Residue. Ongoing work in this laboratory has shown that this residue is useful for the enantioselection of cancers.[24] The position of the H194 residue in the human DT-diaphorase active site (Figure 1) results in a hydrogen bonding interaction between the histidine and the carbonyl of the 3-substituent of **1b**, **1c**, and **3a**. Since the *S* enantiomers are more able to undergo this interaction, human histological cancers are more sensitive to the *S* than the *R* enantiomers.[24] In contrast, the H194 residue of rat enzyme is not positioned for hydrogen bonding to the substrate. Figure 5 shows the substrate *S*-**3a** in the human and the rat DT-diaphorase active sites. The absence of this hydrogen bonding interaction in the rat enzyme is manifested

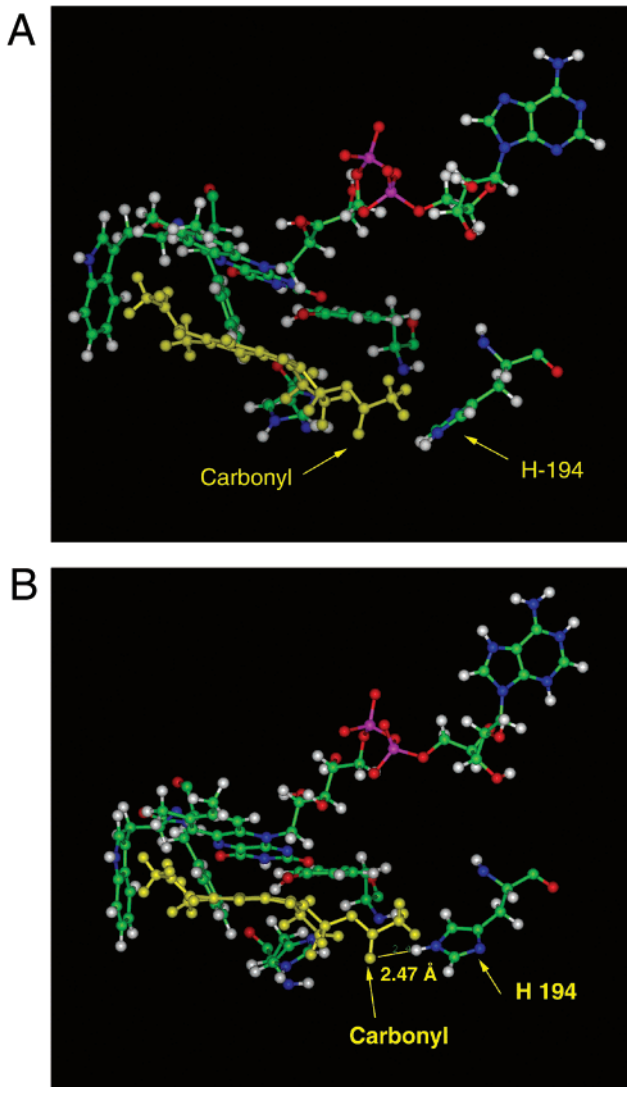

Figure 5. Models of quinone substrate *S*-**3a** bound to rat (A) and human (B) DT-diaphorase active sites. These models illustrate the different position of the histidine residue in the active sites of both enzymes.

by a 20-fold increase in K_M value for *S*-**3a** compared to human enzyme.

It should be pointed out that hydrogen bonding between the 3-substituent of **1** and **3** is not required for substrate activity in human DT-diaphorase. Thus, both the *R* and *S* enantiomers are substrates, with the latter possessing somewhat lower active site energies and therefore higher k_{cat}/K_m values. In some instances, interactions between the 3-substituent and H-194 results in repositioning the substrate. Substrates **1c** and **1d** fall on plot A of Figure 2 as the *R* enantiomers, but the *S* enantiomers fall on plot B.

The findings cited above led to the conclusions discussed below. Although rat and human DT-diaphorases differ in many ways,[19] the H194 residue can readily distinguish the enzymes stereochemically with the appropriate substrate. The H194 residue can influence the position of the quinone substrate in the active site resulting in formation of one of two Michael anions. Cancer enantioselection relies on the H194 residue in human DT-diaphorase,[24] and rat enzyme is therefore unsuitable for substrate specificity determination of candidate compounds.

Conclusions

Previous reports have dealt with the modeling of quinone substrates into the DT-diaphorase active site.[19,20,28] The present study does likewise and also shows that quantitative relationships of predictive value can be developed from DT-diaphorase models. A series of benzimidazole-based quinone substrates were modeled into the active site of human NSC 460 DT-diaphorase and minimized. The models and calculations lead to the following conclusions:

The measured values of the k_{cat}/K_m were correlated with the minimized energy to afford two linear plots reflecting two possible Michael hydride transfer processes. Hydride transfer by Michael addition to quinones was suggested as a DT-diaphorase reduction mechanism[19] and documented in a chemical system.[27] Most complex quinone substrates (mitomycin C and EO9) may likewise undergo one of two possible Michael additions, depending on their position in the active site. It is concluded that the "duroquinone" structure is not preserved in all quinone substrates due to steric interactions elsewhere in the DT-diaphorase active site. With two hydride transfer processes possible, repositioning of substrates will still result in reduction.

In a previous study, it was surprising to observe that rat DT-diaphorase could reduce polycyclic quinone substrates such as **4b**,**c**.[14] The human DT-diaphorase does likewise and even reduces the larger substrate **5**. Minimized structures of human DT-diaphorase bound to **4b**,**c** and **5** are very stable with two rings of the pentacyclic systems sandwiched between W-105 and F-106. These amino acid residues very likely intercalate polycyclic quinones in the DT-diaphorase active site to facilitate reductive detoxification.[12,13]

Finally, the H194 residue of human DT-diaphorase functions as a hydrogen bond donor to the carbonyl of the 3-acetamido and carbamido substituents of quinone series **1** and **3**.

Experimental Section

All analytically pure compounds were dried under high vacuum in a drying pistol over refluxing toluene. Elemental analyses were run at Atlantic Microlab, Inc., Norcross, GA. Elemental analyses are reported for purified final products namely, **1d**. All TLCs were performed on silica gel plates using a variety of solvents and a fluorescent indicator for visualization. IR spectra were taken as thin films and the strongest absorbances reported. ^{1}H NMR and ^{13}C NMR spectra were obtained from a 300 MHz and a 75 MHz spectrometer, respectively, unless otherwise specified. All chemical shifts are reported relative to TMS.

3-*N*,*N*′-Dimethylcarbamido-6-aziridinyl-2,3-dihydro-7-methyl-1*H*-pyrrolo[1,2-*a*]benzimidazole-5,8-dione (1d). A solution of 3-amino-6-aziridinyl-2,3-dihydro-7-methyl-1*H*-pyrrolo[1,2-*a*]benzimidazole-5,8-dione **1a** (35 mg, 0. 136 mmol), anhydrous *p*-dioxane (9 mL), triethylamine (5 mL), and *N*,*N*-dimethylcarbomyl chloride (0.15 mL, 1.6 mmol) was placed under nitrogen. The reaction was stirred at 60 °C for 26 h and then concentrated in vacuo. The residue was dissolved in 8% methanol in methylene chloride and purified by flash column chromatography using 8% methanol in methylene chloride as the eluent. Evaporation of solvent gave a dark red solid which was recrystallized from chloroform/hexane: 26.8 mg (60%) yield; mp >260 °C; TLC (10% methanol in chloroform) R_f = 0.64; IR (KBr pellet) 3306, 3001, 2926, 2361, 1668, 1635, 1570, 1518, 1379, 1313, 1215, 1138 cm^{-1}; ^{1}H NMR ($CDCl_3$) δ 6.39 (1H, d, J = 6.6 Hz, amide proton), 5.25−5.22 (1H, m, 3-methine), 4.30−4.23 and 4.06−3.99 (2H, 2m, 1-methylene), 3.11−

3.01 and 2.92−2.68 (2H, 2m, 2-methylene), 2.95 (6H, s, 2-CH_3), 2.38 (4H, s, aziridinyl protons), 1.97 (3H, s, 7-methyl); MS (EI) *m*/*z* 329 (M^+). The *R* and *S* enantiomers of **1d** were prepared from the enantiomerically pure **1a**. Anal. Calcd ($C_{16}H_{19}N_5O_3 \cdot 1.65\ H_2O$) C, H, N.

(*S*)-(−) and (*R*)-(+)-4-Acetamido-8-methyl-1,2,3,4-tetrahydropyrido[1,2-*a*]benzimidazole (6) were prepared from (L)- and (D)-2,5-diaminopentanoic acid, respectively, by the general three-step procedure described below using either the indicated portions of reactants or proportional amounts thereof.

To a refluxing solution of 5 g (0.03 mol) of 2,5-diaminopentanoic acid in 50 mL of water was added 13.5 g (0.06 mol) of $CuCO_3 \cdot Cu(OH)_2$, and the resulting mixture was refluxed for 3 h. The reaction mixture was filtered hot, and the precipitate was washed 2× with 20 mL portions of hot water. The deep blue filtrate was allowed to cool to room temperature, and (10 g, 0.12 mol) $NaHCO_3$ was added to the solution. To the stirred mixture was added a solution of 9.6 g (0.04 mol) of 3-bromo-4-nitrotoluene in 96 mL of acetone. The resulting solution was refluxed overnight during which a dark green solid separated out from the reaction mixture. The precipitate was washed with water, acetone, and diethyl ether sequentially to yield 1.86 g of a dark green solid. The precipitate was suspended in 60 mL of boiling water, and then hydrogen sulfide gas was bubbled through it for 25 min with continued heating. The mixture was then stirred for additional 10 min, treated with 60 mL of 6 N HCl, and filtered hot. The filtrate was cooled to room temperature and then neutralized to pH 7 by dropwise addition of 4 N NaOH. The neutralized mixture was left in the refrigerator overnight during which yellow precipitate was obtained: 1.04 g (13%) yield.

The yellow precipitate was suspended in 120 mL of methanol containing 4 mL of 4 N HCl. Nitrogen was bubbled through this solution for 10 min and then 420 mg of 5% Pd on carbon was added, and the reaction mixture was hydrogenated at 50 psi overnight. The reaction mixture was filtered through sintered funnel, and the black solid was washed 2× with 20 mL portions of methanol. The solvent was removed under reduced pressure to afford an off-white residue.

The residue obtained above was immediately dissolved in 160 mL of 4 N HCl, and the resulting solution was refluxed for 16 h. At the end of the reaction time, the reaction mixture was neutralized to pH 6−7 with cooling on an ice bath. To this mixture were added 150 mL of acetic anhydride and 50 mL of acetic acid, and the reaction mixture was stirred for 6 h. The solution was neutralized with saturated $NaHCO_3$ solution and then extracted 3× with 60 mL portions of chloroform. The organic layer was dried over sodium sulfate and then concentrated in vacuo to yield either (*S*)-**6** or (*R*)-**6** as light brown solids:

(*S*)-**6**: Yield 67%; mp (dec) 243−245 °C; TLC (10% methanol in chloroform) R_f = 0.48; IR (KBr pellet) 3448, 3304, 2953, 2922, 2858, 2364, 1639, 1541, 1425, 1309, 1261, 1153 cm^{-1}; ^1H NMR ($CDCl_3$) δ 7.59−7.57 (1H, d, 6-aromatic), 7.12−7.10 (1H, d, 7-aromatic), 7.10 (1H, s, 9-aromatic), 5.22−5.15 (1H, m, 4-methine), 4.21−4.16 and 3.96−3.86 (2H, 2m, 1-methylene), 2.71−2.66, 2.29−2.25, 2.19−2.10 and 1.78−1.71 (4H, 4m, 2-methylene and 3-methylene), 2.49 (3H, s, 8-CH_3), 2.11 (3H, s, methyl); MS (EI) *m*/*z* 243 (M^+), 200 ($M^+ - COCH_3$). Rotation: $S(-)$ $[\alpha]_D^{25} = -54°$ (c = 1.8, EtOH).

(*R*)- **6**: Yield 38%; mp (dec) 251−253 °C; TLC (10% methanol in chloroform) R_f = 0.44; IR (KBr pellet) 3448, 3290, 2957, 2862, 2359, 1716, 1637, 1547, 1427, 1271, 1261, 1153 cm^{-1}; ^1H NMR ($CDCl_3$) δ 7.617−7.587 (1H, d, 6-aromatic), 7.123−7.099 (1H, d, 7-aromatic), 7.112 (1H, s, 9-aromatic), 5.19−5.12 (1H, m, 4-methine), 4.22−4.16 and 3.97−3.87 (2H, 2m, 1-methylene), 2.78−2.72, 2.28−2.21, 2.20−2.16 and 1.74−1.61 (4H, 4m, 2-methylene and 3-methylene), 2.49 (3H, s, 8-CH_3), 2.10 (3H, s, methyl); MS (EI) *m*/*z* 243 (M^+), 200 ($M^+ - COCH_3$). Rotation: $R(+)$ $[\alpha]_D^{25} = +50°$ (c = 2.2, EtOH).

4-Trifluoroacetamido-8-methyl-1,2,3,4-tetrahydropyrido[1,2-*a*]benzimidazole (7) was prepared from **6** by the following two-step procedure.

The deacetylation was carried out by dissolving 195 mg (0.8 mmol) of **6** in 400 mL of 1.2 N hydrochloric acid and refluxing for 12 h. The solvent was removed in vacuo, and the off-white residue was dried under vacuum for 2 h. Trifluoroacetylation was carried out by dissolving the dried product in 8 mL of trifluoroacetic acid followed by addition of 8 mL of trifluoroacetic anhydride. The reaction mixture was stirred for 20 min at room temperature and then poured into 100 mL of 0.1 M pH = 7 phosphate buffer. This solution was extracted 3× with 35 mL portions of ethyl acetate, and the organic extracts were then washed 2× with 100 mL portions of saturated sodium bicarbonate and dried over anhydrous sodium sulfate. The dried organic extract was concentrated to a residue that was recrystallized from ethyl acetate/hexane to yield 160 mg (67% yield) of a yellow solid: mp 195−198 °C; TLC (10% methanol in chloroform) R_f = 0.8; IR (KBr pellet) 3443, 2924, 2922, 2362, 1685, 1456, 1211, 1145 cm^{-1}; ^1H NMR ($CDCl_3$) δ 8.04 (1H, bs, amide proton) 7.58−7.55 (1H, d, 6-aromatic), 7.13−7.10 (1H, d, 7-aromatic), 7.06 (1H, s, 9-aromatic), 5.21−5.13 (1H, m, 4-methine), 4.19−4.13 and 3.95−3.86 (2H, 2m, 1-methylene), 2.78−2.69, 2.38−2.26, 2.22−2.15 and 1.94−1.81 (4H, 4m, 2-methylene and 3-methylene), 2.49 (3H, s, 8-CH_3); MS (EI) *m*/*z* 297 (M^+), 200 ($M^+ - COCF_3$). Rotation: $S(-)[\alpha]_D^{25} = -15.6°$ (c = 1.6, EtOH) and $R(+)[\alpha]_D^{25} = +10.8°$($c$ = 0.74, EtOH).

7-Bromo-4-trifluoroacetamido-8-methyl-6-nitro-1,2,3,4-tetrahydropyrido[1,2-*a*]benzimidazole (8) was prepared from **7** by the following two-step procedure.

To a solution of 180 mg (0.61 mmol) of **7** in 10 mL of acetic acid was added 0.6 mL of 0.8 M bromine in acetic acid. The resulting mixture was stirred for 25 min at room temperature and then quenched by addition of 200 mL of 0.1 M pH = 7 phosphate buffer. The resulting mixture was extracted 3× with 35 mL portions of ethyl acetate. The organic extracts were combined and washed 2× with 60 mL portions of saturated sodium bicarbonate and then dried over anhydrous sodium sulfate. The organic layer was concentrated, and residue was recrystallized from ethyl acetate/hexane to afford 154 mg of a pale yellow solid (67% yield): TLC (10% methanol in chloroform) R_f = 0.47; IR (KBr pellet) 3277, 3095, 2957, 2567, 2361, 1703, 1560, 1450, 1188 cm^{-1}; ^1H NMR ($CDCl_3$) δ 7.98 (1H, bs, NH proton), 7.87 (1H, s, 6-aromatic proton), 7.13 (1H, s, 9-aromatic proton), 5.18−5.13 (1H, m, 4-methine), 4.18−4.12 and 3.98−3.89 (2H, 2m, 1-methylene), 2.75−2.68, 2.38−2.29, 2.27−2.18 and 1.97−1.93 (4H, 4m, 2-methylene and 3-methylene), 2.51 (3H, s, 8-CH_3); MS (EI) *m*/*z* 377 and 375 (M^+, ^{81}Br and ^{79}Br), 280 and 278 ($M^+ - COCF_3$).

The 7-bromo-4-trifluoroacetamido-8-methyl-1,2,3,4-tetrahydropyrido[1,2-*a*]benzimidazole (154 mg, 0.41 mmol) obtained above was added slowly to chilled fuming nitric acid (10 mL) with continuous stirring on an ice−salt bath. To this mixture, acetic anhydride (0.6 mL) was added, and the reaction mixture was stirred in an ice bath for another 5 min. The ice−salt bath was removed, and the reaction mixture was stirred at room temperature for 90 min. The reaction mixture was then poured into 200 mL of ice water followed by neutralization with saturated sodium bicarbonate solution. The aqueous layer was extracted 3× with 60 mL portions of ethyl acetate, and the extracts were dried over anhydrous sodium sulfate. The solvent was removed in vacuo, and the yellow residue was recrystallized using ethyl acetate and hexane to yield 116 mg of a pale yellow solid (67% yield): mp 199−201 °C; TLC (10% methanol in chloroform) R_f = 0.62; IR (KBr pellet) 3229, 3055, 2957, 2928, 2361, 2337, 1720, 1543, 1375, 1213, 1161, 1039 cm^{-1}; ^1H NMR ($CDCl_3$) δ 8.34 (1H, bs, NH proton), 7.36 (1H, s, 9-aromatic), 5.19−5.12 (1H, m, 4-methine), 4.29−4.24 and 4.11−4.01 (2H, 2m, 1-methylene), 2.91−2.86, 2.42−2.36, 2.26−2.17 and 2.01−1.88 (4H, 4m, 2-methylene and 3-methylene), 2.58 (3H, s, 8-CH_3); MS (EI) *m*/*z* 419 (M^+), 373 ($M^+ - NO_2$), 351, 333, 323, 305, 294, 278, 224, 198. Rotation: $S(-)[\alpha]_D^{25} = -15°$ (c = 0.88, EtOH) and $R(+)[\alpha]_D^{25} = +13°$ (c = 0.90, EtOH).

4-Amino-7-aziridinyl-8-methyl-1,2,3,4-tetrahydropyrido-[1,2-*a*]benzimidazole-6,9-dione (2). To a well-stirred solu-

tion of 66 mg (0. 156 mmol) of **8** in 10 mL of ethanol was added 100 mg (2.6 mmol) of sodium borohydride portion wise. The resulting mixture was stirred at room temperature for 1 h. The reaction mixture was then filtered through a sintered glass funnel. The filtrate was concentrated in vacuo and then loaded over a silica column and eluted with 8% methanol in methylene chloride in chloroform. The fraction containing the product was concentrated in vacuo and the residue recrystallized from chloroform/hexane to yield a crude yellow solid (26 mg): yield 51%; R_f = 0.42 (8% methanol in chloroform); ^{1}H NMR ($CDCl_3$) δ 7.31 (1H, s, 9-aromatic), 4.32−4.27 (1H, m, 4-methine), 4.15−4.11 and 4.05−4.01 (2H, 2m, 1-methylene), 2.38−2.34, 2.21−2.05 and 1.84−1.11 (4H, 4m, 2-methylene and 3-methylene), 2.58 (3H, s, 8-CH_3); MS (EI) *m*/*z* 325 (M^+), 309, 296, 279, 249, 198.

The unstable product obtained above(46 mg, 0.14 mmol) was quickly dissolved in 40 mL of methanol, and the resulting solution was hydrogenated in the presence of 5% Pd over carbon (80 mg) at 50 psi for 5 h. The reaction mixture was filtered over sintered glass funnel, and the filter cake was washed 2× with 20 mL portions of methanol. The solvent was removed in vacuo and the residue redissolved in 20 mL of water containing 0.3 g of KH_2PO_4. The resulting mixture was combined with another 20 mL solution containing 1 g of KH_2PO_4 and 0.8 g (3 mmol) of Fremy salt. The reaction mixture was stirred at room temperature for 5 h. The solution was then concentrated under high vacuum and the residue loaded over Bakerbond phenyl reverse-phase column (15 g resin) prepared in water. The unstable aminoquinone was eluted as yellow fraction from the column with water, and the combined fractions were concentrated to dryness. The residue was resuspended in 20 mL of methanol and 0.8 mL of aziridine. The resulting mixture was stirred at room temperature for 5 h. The solution was concentrated in vacuo, and the residue was purified by flash column chromatography using 8% methanol in chloroform as the eluent. The organic fraction was concentrated in vacuo, and the residue was recrystallized from chloroform/hexane to yield a red solid (6.8 mg): yield 18% overall; mp (dec) >235 °C. TLC (10% methanol in chloroform) R_f = 0.41; IR (KBr pellet) 3454, 2935, 2364, 2343, 1676, 1637, 1541, 1381, 1340, 1188 cm^{-1}; ^{1}H NMR ($CDCl_3$) δ 4.46−4.38 and 4.2−4.1 (3H, 3m, 4-methine and 1-methylene), 2.31−2.18, 2.03−1.91 and 1.74−1.66 (4H, 4m, 2-methylene and 3-methylene), 2.39 (4H, s, aziridinyl protons), 2.07 (3H, s, 8-methyl); MS (EI) *m*/*z* 272 (M^+). Anal. Calcd ($C_{14}H_{16}N_2O_4$) C, H, N.

1,3-Bis(piperidino)-4,6-dinitrobenzene (9). To 1.98 g (6.1 mmol) of 1,3-dibromo-4,6-dinitrobenzene in a round-bottom flask was added 4 mL of piperidine dropwise. After completing the addition, the reaction mixture was heated at 90 °C for 12 h. The reaction mixture was then poured over cracked ice and stored in the refrigerator for 4 h. The precipitate was filtered off, and the product was purified by flash chromatography using silica gel with chloroform as eluent. The organic fractions containing the product were combined, and the solvent was removed in vacuo. The resulting solid was recrystallized from chloroform/hexane to yield 1,3-piperidino-4,6-dinitrobenzene **9** as a yellow solid (1.77 g, 86% yield), mp 120−124 °C. TLC (5% methanol in $CHCl_3$) R_f = 0.69; IR (KBr pellet) 2945, 2852, 1601, 1560, 1510, 1446, 1342, 1242, 856 cm^{-1}; ^{1}H NMR ($CDCL_3$) δ 8.67 and 6.27 (2H, 2s, aromatic protons), 3.14−3.11 (8H, t, pyrido protons), 1.78−1.74 (8H, t, pyrido protons), 1.69−1.66 (4H, m, pyrido protons); *m*/*z* 334 (M^+), 317 (M^+ − OH).

6-Nitro-1,2,3,4,8,9,10,11-octahydrodipyrido[1,2-*a*:1′,2′-*a*′]benzo[1,2-*d*:5,4-*d*′]diimidazole (10) was prepared by the four-step procedure outlined below. A solution containing 1.60 g (4.8 mmol) of **9** and 400 mg of 5% Pd on carbon in 200 mL of acetic acid was shaken under 50 psi of H_2 for 12 h. The reaction mixture was filtered through sintered funnel to remove the catalyst. To the filtrate was added 100 mL of acetic anhydride, and the solution was stirred at room temperature for 1.5 h. The solvent was reduced in vacuo to afford an oil, to which 300 mL of diethyl ether was added resulting in crystallization of the product as a white solid: 897 mg (52%) yield; mp 223−226 °C; TLC (5% methanol in chloroform) R_f = 0.2; IR (KBr pellet) 3288, 2939, 2852, 2802, 1658, 1597, 1533, 1504, 1417, 1130, 1111, 1031, 906 cm^{-1}; ^{1}H NMR ($CDCl_3$) 9.06 and 6.89 (2H, 2s, aromatic protons), 8.24 (2H, s, amide protons), 2.76−2.75 (8H, t, pyrido protons), 2.17 (6H, s, methyl protons), 1.72−1.70 (8H, t, pyrido protons), 1.58 (4H, m, pyrido protons) *m*/*z* 358 (M^+), 315 (M^+ − ketene).

To a solution consisting of 6 mL of 96% formic acid and 3 mL of 30% hydrogen peroxide was added the acetylated product prepared as described above (860 mg, 2.4 mmol). The resulting mixture was stirred at 70 °C for 2 h and then cooled to room temperature. The reaction mixture was diluted with 20 mL of water, and the pH of the solution was adjusted to 7 (approximately) with concentrated ammonium hydroxide. The resulting solution was extracted 5× with 20 mL portions chloroform. The dried organic solvent ($NaSO_4$) was removed in vacuo to afford a crude product that was recrystallized from chloroform/hexane: 202 mg (31%) yield; mp 104−108 °C. TLC (10% methanol in chloroform) R_f = 0.23; IR (KBr pellet) 3418, 2949, 1707, 1633, 1446 cm^{-1}; ^{1}H NMR ($CDCl_3$) 7.963 and 7.117 (2H, 2s, aromatic protons), 4.146−4.116 (4H, t, pyrido protons), 3.202−3.171 (4H, t, pyrido protons), 2.207−2.179 (4H, m, pyrido protons), 2.091−2.047 (4H, m, pyrido protons) *m*/*z* 266 (M^+).

To a solution consisting of 4 mL fuming nitric acid and 4 mL of concentrated sulfuric acid cooled in an ice−salt bath to 0 °C was added 190 mg of **5** (0.714 mmol), and the mixture stirred for 15 min. At the end of the reaction time, the mixture was poured over cracked ice and the pH adjusted to 6−6.5 using concentrated ammonium hydroxide. The resulting aqueous solution was extracted 4× with 20 mL portions of chloroform. The chloroform extracts were combined and dried (Na_2SO_4), and then concentrated to afford the crude product. The product was recrystallized using chloroform/hexane to yield a yellow solid: 110 mg (50% yield); mp 230−232 °C dec. TLC (10% methanol in chloroform) R_f = 0.19; IR (KBr pellet) 3431, 2951, 1653, 1496, 1365, 1244, 1028 cm^{-1}; ^{1}H NMR ($CDCl_3$) 7.385 (1H, s, aromatic proton), 4.191−4.151 (4H, t, pyrido protons), 3.265−3.223 (4H, t, pyrido protons), 2.233−2.202 (4H, m, pyrido protons), 2.097−2.061 (4H, m, pyrido protons); MS(EI mode) *m*/*z* 311 (M^+), 281 (M^+ − NO).

1,2,3,4,8,9,10,11-Octahydrodipyrido[1,2-*a*:1′,2′-*a*′]benzo-[1,2-*d*:5,4-*d*′]diimidazole-6, 12-dione(5) was prepared by the two-step procedure outlined below.

A solution consisting of 98 mg (0.32 mmol) of **10**, 50 mg of 5% Pd on carbon, and 50 mL methanol was shaken at 50 psi H_2 for 4 h. The mixture was filtered using sintered funnel, and the filter cake was washed 2× with 20 mL portions of methanol. The filtrate was removed in vacuo and then redissolved in 10 mL of water containing monobasic potassium phosphate (500 mg). To this solution was then added 0.9 g of Fremy salt and 25 mL of 0.1 M monobasic potassium phosphate in water. The resulting reaction mixture was then stirred for 2 h, and the aqueous solution was extracted 3× with 20 mL portions of chloroform. The organic fractions were combined, dried (Na_2SO_4), and then concentrated to a crude solid. The solid was recrystallized from chloroform/hexane to yield a yellowish solid: 34 mg (36% yield); mp > 260 °C; TLC (10% methanol in chloroform) R_f = 0.23; IR (KBr pellet) 3448, 2947, 1678, 1651, 1423, 1294, 1047 cm^{-1}; ^{1}H NMR ($CDCl_3$) δ 4.36−4.32 (4H, t, pyrido protons), 3.02−2.97 (4H, t, pyrido protons), 2.06−1.94 (8H, m, pyrido protons). *m*/*z* 296 (M^+). Anal. Calcd. ($C_{16}H_{16}N_4O_2 \cdot 0.8H_2O$) C, H, N.

Human and Rat DT-Diaphorase Coordinates. Crystallographic coordinates for rat (1QRD) and human DT-diaphorase (1D4A)[18,19] were obtained from the Protein Data Bank.

The coordinates for rat DT-diaphorase included bound FAD, duraquinone (substrate), and Cibacron blue (inhibitor). The human DT-diaphorase coordinates included FAD as the only bound molecule. For modeling purposes, INSIGHT II from Molecular Simulations, Inc. (San Diego) was used. Rat DT-diaphorase exists as a dimer with two catalytic sites, and human DT-diaphorase exists as a tetramer with four catalytic active sites. All the superimpositions and minimizations were performed on a single monomer unit bearing a single catalytic

active site for rat (1QRD:A) as well as for human DT-diaphorase (1D4A:A). After downloading the PDB coordinates for rat and human DT-diaphorase, hydrogens were added, and the potentials and charges of atoms for the entire monomer were fixed. The FAD cofactor for rat DT-diaphorase had to have the atom potentials assigned. The resulting structure was minimized for 3000 iterations (RMSD = 0.03) using the consistent valence force field (CVFF). Alternatively, the entire protein backbone was fixed after adding hydrogens, and the structure was subjected to steepest descent minimization to an RMS derivative value of less than 0.001 using consistent valence force field. Either minimization method afforded a protein structure suitable for modeling.

Modeling into the DT-Diaphorase Active Site. The substrates for rat and human DT-diaphorase were constructed utilizing fragments available in fragment libraries of BUILDER module. The molecules were constructed and then energy minimized for 500−1000 iterations before superimposing on the enzyme bound substrate (duraquinone) of rat DT-diaphorase. These substrates are mainly heterocycles with short side chains, and conformational searching was not necessary. There are two to four possible ways for the substituted quinone substrates **1**−**5** to be superimposed on the enzyme-bound duroquinone. The optimal binding orientation of the substrate was obtained by superimposing the quinones on duraquinone in all two to four possible orientations. After each superimposition, duraquinone was deleted from the enzyme active site. The potentials for the native structures were fixed, and the superimposed quinone, along with the rat DT-diaphorase and bound FAD, was associated as an assembly and then energy minimized using DISCOVER module. This process was repeated for all two to four possible orientations. The orientation with the lowest energy (van der Waals and electrostatic) was chosen as the optimal enzyme-bound structure. This quinone-rat DT-diaphorase assembly was then utilized as a template for generating models for human enzyme. This was done by superimposing the isoalloxazine ring of the FAD bound cofactor from this assembly unto that of the FAD bound cofactor in the human enzyme. After the superimposition, rat DT-diaphorase enzyme and the rat FAD were removed from the assembly, and the human DT-diaphorase bearing the quinone substrate was made into an assembly and the energy minimized for either 5000 iterations or until an RMSD of 0.05 Å was reached (15 000 to 33 000 iterations).

Optimization of DT-diaphorase bound quinones was obtained using the DOCKING module of INSIGHT II. The consistent valence force field (CVFF) was employed for all DOCKING purposes. The GRID was generated around the active site residues (W-105, F-106, Y-155, H-161, H-194). The rest of the residues of the monomeric enzyme were treated as immovable or rigid area. The optimal binding orientation was achieved by utilizing convergent gradient (Polak-Ribiere) method for 300 iterations. Generally these docked structures were very similar to the minimized structures obtained above.

Kinetics Studies Using Recombinant DT-Diaphorase. Kinetics studies were carried out in 0.05 M pH 7.4 Tris buffer under anaerobic conditions, employing Thunberg cuvettes. A 4.0 mM PBI stock solution was prepared in dimethyl sulfoxide (DMSO). To the top port of the cuvette was added the PBI stock solution, and to the bottom port was added the recombinant DT-diaphorase and NADH stock solutions in Tris buffer. Both portions were purged with argon for 20 min and equilibrated at 30 °C for 10 min. The ports were then mixed, and the reaction was followed at 336 nm for 10 min to obtain initial rates. The final concentrations of the mixture were 0.3 mM NADH, 1.3×10^{-6} to 6.7×10^{-5} M of PBI, and 1.4×10^{-9} M of recombinant DT-diaphorase. To calculate V_{max}, the value of $\Delta\epsilon$ must be obtained. $\Delta\epsilon$ was calculated from the initial and final absorbances for complete PBI reduction; all values are between 8000 and 9000 M^{-1} cm^{-1}. All data were fitted to a Lineweaver−Burke plot from which k_{cat} and K_m were obtained.

Chiral High-Pressure Liquid Chromatography HPLC separations of enantiomers were done on Chirex column (50 × 3.2 mm) from Phenomenex. The detector was set at 285 nm, and the flow rate was adjusted at 0.7 mL/min with the mobile phase consisting of hexane, 1,2-dichloroethane, and ethanol [57:30:13]. Chirex column (00B-3014-RO) was used for the separation of compound **6**. Measured retention time in minutes was as follows: 4.15 for *S*-**6** and 6.26 for *R*-**6**.

Acknowledgment. We wish to thank Professor David Ross for the generous supply of NSC 460 recombinant DT-diaphorase. This work was supported by the National Science Foundation, the National Institutes of Health, and the Arizona Disease Control Commission

References

(1) Rauth, A. M.; Goldberg, Z.; Misra, V. DT-diaphorase: Possible roles in cancer chemotherapy and carcinogenesis. *Oncol. Res.* **1997**, *9*, 339−349.
(2) Rauth, A. M.; Melo, T.; Misra, V. Bioreductive therapies: An overview of drugs and their mechanisms of action. *Int. J. Radiat. Oncol. Biol. Phys.* **1998**, *42*, 755−762.
(3) Stratford, I. J.; Workman, P. Bioreductive drugs into the next millennium. *Anti. Cancer Drug. Des.* **1998**, *13*, 519−528.
(4) Fitzsimmons, S. A.; Workman, P.; Grever, M.; Paull, K.; Camalier, R.; Lewis, A. D. Reductase enzyme expression across the National Cancer Institute Tumor cell line panel: correlation with sensitivity to mitomycin C and EO9. *J. Natl. Cancer Inst.* **1996**, *88*, 259−69.
(5) Siegel, D.; Beall, H.; Senekowitsch, C.; Kasai, M.; Arai, H.; Gibson, N. W.; Ross, D. Bioreductive Activation of Mitomycin C by DT-Diaphorase. *Biochemistry* **1992**, *31*, 7879−7889.
(6) Cummings, J.; Spanswick, V. J.; Tomasz, M.; Smyth, J. F. Enzymology of mitomycin C metabolic activation in tumour tissue − Implications for enzyme-directed bioreductive drug development. *Biochem. Pharmacol.* **1998**, *56*, 405−414.
(7) Naylor, M. A.; Swann, E.; Everett, S. A.; Jaffar, M.; Nolan, J.; Robertson, N.; Lockyer, S. D.; Patel, K. B.; Dennis, M. F.; Stratford, M. R. L.; Wardman, P.; Adams, G. E.; Moody, C. J.; Stratford, I. J. Indolequinone antitumor agents: Reductive activation and elimination from (5-methoxy-1-methyl-4,7-dioxoindol-3-yl)methyl derivatives and hypoxia-selective cytotoxicity in vitro. *J. Med. Chem.* **1998**, *41*, 2720−2731.
(8) Jaffar, M.; Naylor, M. A.; Robertson, N.; Stratford, I. J. Targeting hypoxia with a new generation of indolequinones. *Anti. Cancer Drug. Des.* **1998**, *13*, 593−609.
(9) Skibo, E. S.; Gordon, S.; Bess, L.; Boruah, R.; Heileman, J. Studies of Pyrrolo[1,2-*a*]benzimidazole Quinone DT-Diaphorase Substrate Activity, Topoisomerase II Inhibition Activity, and DNA Reductive Alkylation. *J. Med. Chem.* **1997**, *40*, 1327−1339.
(10) Skibo, E. B. Pyrrolobenzimidazoles in cancer treatment. *Expert Opin. Ther. Pat.* **1998**, *8*, 673−701.
(11) Moran, J. L.; Siegel, D.; Ross, D. A potential mechanism underlying the increased susceptibility of individuals with a polymorphism in NAD(P)H: quinone oxidoreductase 1 (NQO1) to benzene toxicity. *Proc. Natl. Acad. Sci. U.S.A.* **1999**, *96*, 8150−8155.
(12) Jarabak, J.; Harvey, R. G. Studies on 3 Reductases Which Have Polycyclic Aromatic Hydrocarbon Quinones as Substrates. *Arch. Biochem. Biophys.* **1993**, *303*, 394−401.
(13) Swanson, M. S.; Haugen, D. A.; Reilly, C. A.; Stamoudis, V. C. Protection by Uridine Diphosphoglucuronic Acid and Dt-Diaphorase Against the Cytotoxicity of Polycyclic Aromatic- Hydrocarbons Isolated From a Complex Coal-Gasification Condensate. *Toxicol. Appl. Pharmacol.* **1986**, *84*, 336−345.
(14) Schulz, W. G.; Skibo, E. B. Inhibitors of topoisomerase II based on the benzodiimidazole and dipyrroloimidazobenzimidazole ring systems: Controlling DT-diaphorase reductive inactivation with steric bulk. *J. Med. Chem.* **2000**, *43*, 629−638.
(15) Xing, C.; Skibo, E. B.; Dorr, R. T. Aziridinyl Quinone Antitumor Agents based on Indoles and Cyclopent[b]indoles: Structure Activity Relationships for Cytotoxicity and Antitumor Activity. *J. Med. Chem.* **2001**, *44*, 3545−3562.
(16) Craigo, W. A.; LeSueur, B. W.; Skibo, E. B. Design of Highly Active Analogues of the Pyrrolo[1,2-a]benzimidazole Antitumor Agents. *J. Med. Chem.* **1999**, *42*, 3324−3333.
(17) Skibo, E. B.; Islam, I.; Schulz, W. G.; Zhou, R.; Bess, L.; Boruah, R. The Organic Chemistry of the Pyrrolo[1,2-*a*]benzimidazole Antitumor Agents. An Example of Rational Drug Design. *Synlett* **1996**, 297−309.
(18) Beall, H. D.; Mulcahy, R. T.; Siegel, D.; Traver, R. D.; Gibson, N. W.; Ross, D. Metabolism of Bioreductive Antitumor Compounds by Purified Rat and Human DT-Diaphorase. *Cancer Res.* **1994**, *54*, 3196−3201.
(19) Faig, M.; Bianchet, M. A.; Talalay, P.; Chen, S.; Winski, S.; Ross, D.; Amzel, L. M. Structures of recombinant human and mouse NAD(P)H: quinone oxidoreductases: species comparison and structural changes with substrate binding and release. *Proc. Natl. Acad. Sci. U.S.A.* **2000**, *97*, 3177−82.

(20) Li, R.; Bianchet, M. A.; Talalay, P.; Amzel, L. M. The Three-Dimensional Structure of NAD(P)H:Quinone Reductase, a Flavoprotein Involved in Cancer Chemoprotection and Chemotherapy: Mechanism of the Two-Electron Reduction. *Proc. Natl. Acad. Sci. U.S.A.* **1995**, *92*, 8846−880.
(21) Chen, S. A.; Wu, K. B.; Zhang, D.; Sherman, M.; Knox, R.; Yang, C. S. Molecular characterization of binding of substrates and inhibitors to DT-diaphorase: Combined approach involving site-directed mutagenesis, inhibitor-binding analysis, and computer modeling. *Mol. Pharmacol.* **1999**, *56*, 272−278.
(22) Skelly, J. V.; Sanderson, M. R.; Suter, D. A.; Baumann, U.; Read, M. A.; Gregory, D. S. J.; Bennett, M.; Hobbs, S. M.; Neidle, S. Crystal structure of human DT-diaphorase: A model for interaction with the cytotoxic prodrug 5-(Aziridin-1-yl)-2,4-dinitrobenzamide (CB1954). *J. Med. Chem.* **1999**, *42*, 4325−4330.
(23) Phillips, R. M.; Naylor, M. A.; Jaffar, M.; Doughty, S. W.; Everett, S. A.; Breen, A. G.; Choudry, G. A.; Stratford, I. J. Bioreductive activation of a series of indolequinones by human DT- diaphorase: Structure−activity relationships. *J. Med. Chem.* **1999**, *42*, 4071−4080.
(24) Huang, X.; Suleman, A.; Skibo, E. B. Rational Design of Pyrrolo-[1,2-*a*]benzimidazole Based Antitumor Agents Targeting the DNA Major Groove. *Bioorg. Chem.* **2000**, *28*, 324−337.
(25) Fersht, A. R. The Hydrogen Bond in Molecular Recognition. *Trends Biochem. Sci.* **1987**, *12*, 301−304.
(26) Schlegel, B. P.; Ratnam, K.; Penning, T. M. Retention of NADPH-linked quinone reductase activity in an aldo-keto reductase following mutation of the catalytic tyrosine. *Biochemistry* **1998**, *37*, 11003−11011.
(27) Skibo, E. B.; Lee, C. H. Facile Oxidation of Methoxide to Formaldehyde by a Heterocyclic Quinone. *J. Am. Chem. Soc.* **1985**, *107*, 4591−4593.
(28) Cavelier, G.; Amzel, L. M. Mechanism of NAD(P)H: quinone reductase: Ab initio studies of reduced flavin. *Protein Struct. Funct. Genet.* **2001**, *43*, (4), 420−432.

JM0104365